Time-Dependent Thermodynamics during Early Electron Transfer in Reaction Centers from *Rhodobacter sphaeroides*†

Jeffrey M. Peloquin, JoAnn C. Williams, Xiaomei Lin, Rhett G. Alden,‡ Aileen K. W. Taguchi, James P. Allen, and Neal W. Woodbury*

Department of Chemistry and Biochemistry and the Center for the Study of Early Events in Photosynthesis, Arizona State University, Tempe, Arizona 85287-1604

Received January 27, 1994; Revised Manuscript Received April 19, 1994®

ABSTRACT: The temperature dependence of fluorescence on the picosecond to nanosecond time scale from the reaction centers of *Rhodobacter sphaeroides* strain R-26 and two mutants with elevated P/P^+ midpoint potentials has been measured with picosecond time resolution. In all three samples, the kinetics of the fluorescence decay is complex and can only be well described with four or more exponential decay terms spanning the picosecond to nanosecond time range. Multiexponential fits are needed at all temperatures between 295 and 20 K. The complex decay kinetics are explained in terms of a dynamic solvation model in which the charge-separated state is stabilized after formation by protein conformational changes. Many of these motions have not had time to occur on the time scale of initial electron transfer and/or are frozen out at low temperature. This results in a time- and temperature-dependent enthalpy change between the excited singlet state and the charge-separated state that is the dominant term in the free energy difference between these states. Long-lived fluorescence is still observed even at 20 K, particularly for the high-potential mutants. This implies that the driving force for electron transfer on the nanosecond time scale at low temperature is less than 200 cm^{-1} (25 meV) in R-26 reaction centers and even smaller on the picosecond time scale or in the high-potential mutants. The mechanistic implications of this surprising result are considered, and it is suggested that, at least under certain conditions, electron transfer in the reaction center may be best described as adiabatic, occurring near the strong coupling limit, rather than as a nonadiabatic reaction between vibronically equilibrated states.

The thermodynamic parameters involved in the initial photosynthetic electron-transfer reactions of purple nonsulfur bacteria have been the subject of considerable disagreement over the past decade (Schenck et al., 1982; Woodbury & Parson, 1984; Horber et al., 1986; Goldstein et al., 1988; Ogrodnik et al., 1988). Previous measurements have resulted in relatively small values for the standard free energy change associated with the initial electron-transfer reaction(s), especially when compared to most fast electron-transfer reactions in model systems [e.g., Closs and Miller (1988)]. The variation between different measurements of the value of the standard free energy gap for electron transfer between the initial excited singlet state and the first fully populated charge-separated state is significant; values have been reported between -970 cm^{-1} (-120 meV) and -2100 cm^{-1} (-260 meV). This variation in the reported driving force is equivalent to more than 2 orders of magnitude variation in the equilibrium constant for the reaction.

The lack of a detailed understanding of the driving force and its temperature dependence adds considerably to the confusion concerning the mechanism of the initial charge-separation reaction. If the free energy gap between the initial excited singlet state and the state in which an electron has been transferred to the bacteriopheophytin is as small as -970 cm^{-1} ($k_{forward}/k_{backward} = 100$), then the effects of back reactions on kinetic models for electron transfer may be significant, particularly in models involving intermediate charge-separated states (Holzapfel et al., 1989; Chan et al., 1991).

Each of the methods that have been used to measure the standard free energy of the initial electron-transfer event probe a particular intermediate in the electron-transfer pathway. Scheme 1 summarizes the intermediate states and kinetic time constants thought to be involved in the early electron-transfer reactions. P is a dimer of bacteriochlorophylls,[1] and P* is the lowest excited singlet state of the dimer. Electron transfer results in the formation of the state $P^+B_AH_A^-Q_A$ (abbreviated as $P^+H_A^-$) within about 3.5 ps, where B_A is a monomer bacteriochlorophyll, H_A is a monomer bacteriopheophytin, and Q_A is a quinone. A subsequent reaction results in electron transfer to the quinone in about 200 ps [for reviews, see Kirmaier and Holten (1987, 1993), Feher et al. (1989), and Parson (1991)].

The X-ray crystal structures of the reaction centers from both *Rhodopseudomonas viridis* and *Rhodobacter sphaeroides* show that B_A resides roughly between P and H_A (Allen et al., 1987; Chang et al., 1991; Deisenhofer et al., 1984). It is unclear precisely what role this bacteriochlorophyll monomer

† This work was supported by Grants DMB91-58251 and MCB 9219378 from the National Science Foundation, Grants GM41300 and GM45902 from the National Institutes of Health, and a Postdoctoral Fellowship in Plant Biology, DIR-9104322, from the NSF. Instrumentation was purchased with funds from NSF Grant DIR-8804992 and Department of Energy Grants DE-FG-05-88-ER75443 and DE-FG-05-87-ER75361. This is publication No. 200 from the Arizona State University Center for the Study of Early Events in Photosynthesis. The center is funded by DOE Grant DE-FG-88-ER13969 as part of the USDA/DOE/NSF Plant Science Centers Program.

* Corresponding author.

‡ Present address: Department of Biochemistry, University of Washington, Seattle WA 98195.

® Abstract published in *Advance ACS Abstracts,* June 1, 1994.

[1] Abbreviations: P, bacteriochlorophyll dimer; B, bacteriochlorophyll monomer; H, bacteriopheophytin monomer; EDTA, ethylenediaminetetraacetic acid; Tris, tris(hydroxymethyl)aminomethane; ns, nanosecond; ps, picosecond; fs, femtosecond; *Rps.*, *Rhodopseudomonas*; *Rb.*, *Rhodobacter.*

0006-2960/94/0433-8089$04.50/0

Scheme 1

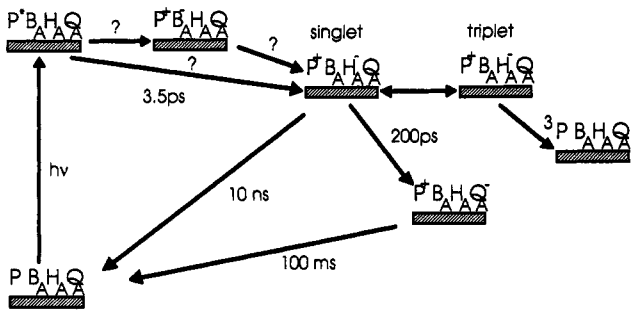

plays in electron transfer, though different mechanistic roles have been proposed (Kirmaier & Holten, 1987, 1993; Parson & Warshel, 1987; Warshel & Parson, 1987; Michel-Beyerle et al., 1988; Holzapfel et al., 1989; Chan et al., 1991; Hamm et al., 1993).

Removal or prereduction of Q_A blocks electron transfer beyond the state $P^+H_A^-$. The weakly coupled spins of the ion radical electrons in this state can dephase and form a charge-separated state with triplet character (Scheme 1). Charge recombination from this state forms the triplet of P, ^3P. Measurement of the triplet yield and decay time as functions of magnetic field strength and temperature is the basis for one of the methods that has been used to determine the thermodynamic parameters of initial electron transfer (Goldstein et al., 1988; Ogrodnick et al., 1988). Because ^3P is thought to decay via the triplet and singlet forms of $P^+H_A^-$ to the ground state, the rate of ^3P decay depends on the rate of intersystem crossing and the equilibrium constant between ^3P and $P^+H_A^-$. Application of a magnetic field splits the triplet levels and decreases the rate of the intersystem crossing. This perturbation can be used to probe the free energy difference between ^3P and $P^+H_A^-$. Using the ^3P energy (Shuvalov & Parson, 1984; Takiff & Boxer, 1988) and the energy of P* from the zero–zero transition energy, the standard free energy difference between P* and $P^+H_A^-$ has been calculated to be about -2100 cm^{-1} (Goldstein et al., 1988; Ogrodnik et al., 1988).

The other primary method for estimating the standard free energy gap for the initial electron transfer involves time-resolved fluorescence measurements. If the free energy difference between P* and $P^+H_A^-$ is small enough, then some small concentration of P* will be present throughout the lifetime of $P^+H_A^-$ due to thermal repopulation of the excited singlet state. Consequently, changes in the concentration of P* with time on the picosecond to nanosecond time scale will depend on the intrinsic lifetimes of P* and $P^+H_A^-$ and on any changes in the free energy gap between P* and $P^+H_A^-$ with time.

Direct measurements of the fluorescence on the femtosecond and picosecond time scales have shown a prominent fluorescence component that decays with essentially the same 3-ps time constant as the charge separation forming $P^+H_A^-$ (Muller et al., 1992; Du et al., 1992; Hamm et al., 1993). These studies also reveal fluorescence components with time constants of 10–100 ps which have amplitudes markedly reduced compared to the amplitude of the prompt fluorescence. Removal or prereduction of the quinones results in yet longer fluorescence components with time constants between 100 ps and 10 ns and even smaller initial amplitudes (Schenck et al., 1982; Sebban & Moya, 1983; Woodbury & Parson, 1984; Horber et al., 1986; Taguchi et al., 1992; Williams et al., 1992a). The free energy difference between P* and $P^+H_A^-$ can be estimated by comparing the total amplitude of the long-lived fluorescence to the initial amplitude of the fluorescence just after P* formation, assuming that the various kinetic components represent a series of thermodynamically distinct forms of $P^+H_A^-$ and that equilibrium with the excited state is maintained at all times (Schenck et al., 1982; Woodbury & Parson, 1984; Taguchi et al., 1992; Williams et al., 1992a).

The potential advantage that the fluorescence measurements have over other methods is that fluorescence can be measured on the time scale of electron transfer, while methods involving triplet P formation utilize measurements made in the tens of nanoseconds to microseconds time range. Fluorescence decay measurements on the nanosecond time scale have given values between -1290 and -1450 cm^{-1} for the standard free energy gap between P* and $P^+H_A^-$ (Schenck et al., 1982; Woodbury & Parson, 1984). More recent fluorescence measurements with a time resolution of roughly 10 ps have yielded a standard free energy gap for this reaction at room temperature of about -970 cm^{-1} [Williams et al., 1992a; similar fluorescence decays have been obtained by Muller et al. (1992), though they analyzed them somewhat differently].

One of the most peculiar and least understood aspects of the long-lived fluorescence from reaction centers in which electron transfer to Q_A is blocked is its temperature dependence. Because the long-lived fluorescence is thought to result from a thermal repopulation of P*, one might expect the amount of the long-lived fluorescence to decrease dramatically with decreasing temperature. A 20–30% decrease in the total amplitude of the long-lived fluorescence is observed between 295 and 270 K. However, between 270 and 200 K the total long-lived fluorescence increases by nearly a factor of 3. Below 200 K, the amplitude of the long-lived fluorescence does decrease, but not as rapidly as would be expected for an entirely enthalpic reaction (Woodbury & Parson, 1984). The unexpected dependence of the amplitude of the fluorescence on temperature is most clearly seen in the slowest (roughly 10 ns) exponential component (Woodbury & Parson, 1984). It is this fluorescence component that has the same magnitude, temperature dependence, and magnetic field dependence as the transient absorption changes associated with the state $P^+H_A^-$ (Schenck et al., 1982; Woodbury & Parson, 1984). These observations strongly support the concept that this fluorescence component arises from a charge-recombination reaction in $P^+H_A^-$ resulting in thermal repopulation of P*.

The shorter-lived fluorescence components display a less pronounced increase in amplitude with decreasing temperature between 270 and 200 K. In addition, the amplitude of these components does not decrease as rapidly below 200 K as does the 10-ns component. In fact, even at 80 K the shorter-lived components of the delayed fluorescence still have significant amplitudes (Woodbury & Parson, 1984). If these components are due to charge recombination, then their weak temperature dependence implies either a very small enthalpy change for the initial electron transfer with a large entropic component for temperatures below 270 K (Woodbury & Parson, 1984) or a temperature-dependent enthalpy. Results based on measurements of the lifetime and yield of ^3P (Ogrodnik et al., 1988; Goldstein et al., 1988) have indicated that the free energy between P* and $P^+H_A^-$ is predominantly of enthalpic origin.

Measurements of the long-lived fluorescence under quinone-reducing conditions have also been performed on whole photosynthetic membranes from a variety of purple nonsulfur bacteria (Woodbury & Parson, 1984; Sebban & Moya, 1983; Ogrodnik et al., 1988). The standard free energy gap calculated for the P* to $P^+H_A^-$ reaction and the temperature dependence of the long-lived fluorescence are very similar to those found in isolated reaction centers. In addition, Booth

et al. (1991) have performed similar time-resolved fluorescence measurements on photosystem II reaction centers from higher plants. Their results, in terms of both the relative magnitude and the temperature dependence of the long-lived fluorescence, are strikingly similar to those obtained for the bacterial system. Similar fluorescence decay kinetics have also been obtained using Fe-S type reaction centers from *Heliobacillus mobilis* (Kleinherenbrink et al., 1994). These observations argue for the concept that the long-lived fluorescence and its unusual temperature dependence are not merely artifacts of the particular preparation or strain used, but instead are indicators of some general property of photosynthetic electron transfer.

Though the properties of the long-lived fluorescence from reaction centers may be general and important, they are poorly understood. This is particularly true for the fastest (10–100 ps) components of the fluorescence, which dominate the calculation of the standard free energy, enthalpy, and entropy changes for the initial electron-transfer reaction. The unexpected properties of the fluorescence decay, particularly at low temperature, warrant further characterization and interpretation.

It has previously been postulated that protein conformational changes resulting in relaxation of the state $P^+H_A^-$ may be important in the description of the fluorescence decay at times greater than a few hundred picoseconds (Woodbury & Parson, 1984), but the complexity of the decay of P* at earlier times is typically rationalized by the involvement of other charge-separated states [Hamm et al., 1993; also discussed in Muller et al. (1992)] or by the presence of a static distribution of reaction center conformations (Du et al., 1992; Muller et al., 1992; Kirmaier & Holten, 1990). In this report, the complicated decay kinetics of P* are reexamined using picosecond time-resolved fluorescence spectroscopy and analyzed in terms of dynamic solvation of the charge-separated state as a function of time. In addition, to better characterize the relationship between the long-lived fluorescence and the relative free energy of $P^+H_A^-$, two *Rb. sphaeroides* reaction center mutants are examined that show elevated steady-state P/P^+ midpoint potentials (Williams et al., 1992a,b). The fluorescence decay from these high-potential reaction centers is compared to that from R-26 reaction centers as a function of time and temperature.

MATERIALS AND METHODS

Bacterial Strains and Reaction Center Isolation. R-26, a carotenoidless mutant of *Rhodobacter sphaeroides*, was grown photoheterotrophically, and reaction centers were isolated following the procedure of Feher and Okamura (1978). The construction of the single-site-directed mutant containing a leucine to histidine change at L131, LH(L131), and the double-site-directed mutant containing a leucine to histidine change at L131 and a leucine to histidine change at M160, LH(L131) + LH(M160), as well as the microaerobic growth of these mutants and the subsequent reaction center isolation, has been described previously (Williams et al., 1992a,b).

For some experiments with R-26 reaction centers, more rigorous isolation procedures were employed in order to obtain very high purity samples. This involved first the normal R-26 reaction center isolation procedure (Feher & Okamura, 1978) followed by an additional fast protein liquid chromatography (FPLC, Pharmacia) step using a tertiary amine column (Western Analytical).

Time-Correlated Single-Photon Counting Measurements. Fluorescence experiments were carried out on quinone-reduced reaction centers suspended in 50 mM Tris-HCl (pH 8.0), 1 mM EDTA, and 0.05% Triton X-100 and diluted 2:1 (v/v) with glycerol (final OD at 860 = 1.0 in a 1-cm path length cell). Dithionite was added to a final concentration of 5 mM, and the sample was placed in a 1-mm path length sample cell, which was mounted on the cold tip of an APD helium displex refrigerator and cooled to the required temperatures. The time-correlated single-photon counting apparatus has been described previously (Gust et al., 1990; Taguchi et al., 1992). For this work, approximately 10-ps excitation pulses at 3.8 MHz from a cavity-dumped, synchronously pumped, styryl-9 dye laser at 860 nm (Spectra Physics) were used. The dye laser was pumped by an Antares mode-locked Nd:YAG laser (Coherent). For quinone-reduced reaction centers, approximately 50–100 mW/cm^2 excitation light was used. The emission was passed through a 0.25-m subtractive monochromator (Instruments SA) with a spectral bandwidth of ±8 nm. The emission was detected by a microchannel plate photomultiplier tube with an S1 photocathode (Hamamatsu) for enhanced near-infrared sensitivity. The timing circuitry and analysis software have been described elsewhere (Gust et al., 1990). The full width at half-maximum of the instrument response function (light scattered from the sample at the excitation wavelength) was 70–90 ps.

Fluorescence decays were analyzed by fitting to a sum of exponential decay terms convoluted with the measured instrument response function. This was done either at single measurement wavelengths or simultaneously to data taken at several emission wavelengths (Taguchi et al., 1992). Reduced χ^2 errors for the fits presented range from 1.0 to 1.2.

RESULTS

Time-Resolved Fluorescence from Rb. sphaeroides Strain R-26 Reaction Centers. Figure 1A shows the fluorescence decay of *Rb. sphaeroides* R-26 reaction centers at 295, 100, and 20 K. At 295 K, less than 5% of the initial (prompt) fluorescence amplitude remains after 10 ps, which is the approximate time resolution of the time-correlated single-photon counting apparatus used for these measurements. What does remain on longer time scales cannot be described by a single-exponential decay, having components ranging from 100 ps to several nanoseconds. This is consistent with previously measured fluorescence decay curves for bacterial reaction centers (Schenck et al., 1982; Sebban & Moya, 1983; Woodbury & Parson, 1984; Muller et al., 1992; Taguchi et al., 1992; Williams et al., 1992a). Table 1 shows the results of fitting the fluorescence decays at 295, 100, and 20 K to a sum of four exponential decay components using a global (multiwavelength) analysis of fluorescence decay between 880 and 940 nm. In this analysis the decay curves at seven wavelengths were fit simultaneously, requiring that the same four kinetic rate constants describe the data at all wavelengths (Taguchi et al., 1992). The use of a smaller number of exponential decay components resulted in a statistically inferior fit. The amplitudes and time constants calculated compare well with previously published values (Muller et al., 1992; Taguchi et al., 1992; Williams et al., 1992a). The amount of the several-nanosecond decay component in Table 1 first increases between 295 and 100 K and then diminishes by at least 30-fold between 100 and 20 K, consistent with previous measurements on longer time scales (Schenck et al., 1982; Woodbury & Parson, 1984). The amplitudes of the two subnanosecond components of fluorescence both increase with decreasing temperature all the way from 295 to 20 K, though the extent of the increase shown in Table 1 is somewhat exaggerated due to the fact that the amplitudes in this table

Table 1: Global Exponential Fits of the Fluorescence Decay Curves in Figure 1[a]

sample	temp (K)	τ_1 (ps)	A_1	τ_2 (ps)	A_2	τ_3 (ps)	A_3	τ_4 (ps)	A_4	τ_5 (ps)	A_5
R-26	295	8.0	970	96	24	766	4	4622	2		
R-26	100	12.5	937	109	48	651	12	5130	3		
R-26	20	17.3	706	100	273	426	19	3706	0.1		
LH(L131)	295	23.9	878	123	90	784	22	3180	10		
LH(L131)	130	49.0	761	177	210	780	22	4901	6		
LH(L131)	20	43.2	658	135	320	623	20	4097	2		
double	295	38.1	698	163	224	649	67	2250	12		
double	120	46.2	469	268	413	747	107	4374	10		
double	20	3.1	815	129	63	363	99	718	24	6000	0.1

[a] The fluorescence amplitudes are given for the fluorescence decay taken at 920 nm and normalized such that the sum of A_i = 1000.

Table 2: Exponential Fitting of 16-ns Fluorescence Decay Traces at 920 nm and 295 K

sample	τ_1 (ps)	A_1	τ_2 (ps)	A_2	τ_3 (ps)	A_3	τ_4 (ps)	A_4	τ_5 (ps)	A_5
R-26	12.9	974	154	20	1411	4	7132	2		
LH(L131)	30.7	940	252	41	1424	14	5130	4		
double	38.1	682	171	201	501	85	1720	27	5110	5

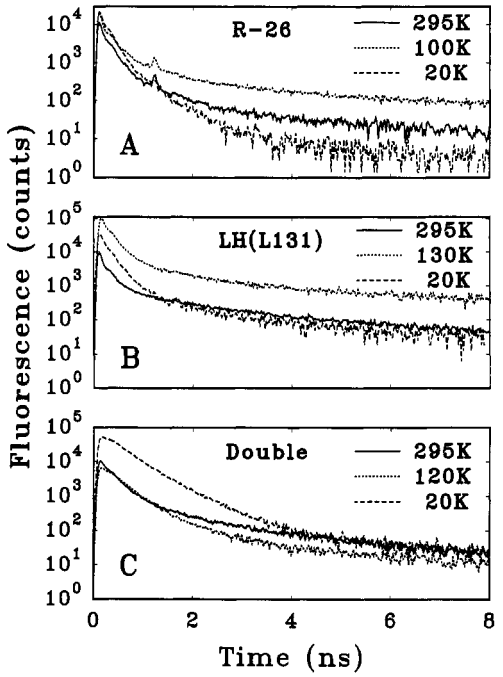

FIGURE 1: Time-correlated single-photon counting fluorescence decay profiles from isolated reaction centers (A) from *Rb. sphaeroides* strain R-26, (B) from the *Rb. sphaeroides* mutant LH(L131), and (C) from the *Rb. sphaeroides* double mutant [LH(L131) + LH-(M160)]. For each sample, photon counts were accumulated in 2000 channels covering 10 ns. The value shown at each time is the total number of photons detected in the corresponding 5-ps interval, displayed on a log scale. Data at three different temperatures are shown as indicated. In each case excitation was at 860 nm and detection was at 900 nm. Similar results were obtained for data collected throughout the 880–940-nm region. Sample conditions and other details of the apparatus are given in Materials and Methods.

were normalized such that they always sum to 1000, and the amplitude of the fastest component determined by the fit is inaccurate since the lifetime of this component is shorter than the time resolution of the apparatus (see below).

There is no particular reason to believe that the individual exponential decay components presented in Table 1 represent kinetically distinct intermediate states of the system. The amplitudes and rate constants presented in Tables 1 and 2 should be viewed simply as a convenient mathematical description of the fluorescence data that removes the instrument response function. The decay times of all of the fluorescence decay components depend on the time scale over which the experiment is performed. Table 2 shows the fit to the decay curve when the time range is doubled from 8 to 16 ns. The time constants of all of the fluorescence components increase with the increase in the time range of the experiment. An even longer lifetime for the slowest decay component was reported previously when a 40-ns time scale was used for the measurement (Woodbury & Parson, 1984). This is what one would expect if, for example, a large number of steps were involved in the process of P* decay but were not resolved kinetically in the fits due to signal-to-noise limitations. Most of the data analysis was performed on data taken over an 8-ns time range. On this time scale, one can resolve both the fluorescence decay on the tens of picoseconds time scale (which is near the time resolution of the apparatus) and the decay on the nanosecond time scale (which is the time scale upon which $P^+H_A^-$ decays to the ground state in quinone-reduced reaction centers). It is important to note that while the fitting parameters that resulted from analyzing the data on different time scales are not identical (Tables 1 and 2), the two fits represent the data equally well on average over the particular time scale used, to within the signal-to-noise characteristics of the data. Since the fits are only used as an accurate means of representing the P* population as a function of time after deconvolution of the instrument response function (see Discussion), the fact that the time constants and preexponential amplitudes of the fits vary with the time scale of the data has no significant effect on the estimation of time-dependent free energy changes performed below.

The fastest component's lifetime (the prompt fluorescence) increases from 8 to 17 ps as the temperature is lowered in the measurements reported here (Table 1). This is in contrast to the measured lifetime of P* by pulse–probe transient absorption measurements of the stimulated emission (Woodbury et al., 1985, 1994; Martin et al., 1986) which show that the lifetime of the excited singlet state decreases by nearly a factor of 2 as the temperature is decreased. This indicates that there are fluorescence decay components on the 10–20-ps time scale whose initial amplitudes increase with decreasing temperature. Decay components on this time scale have been observed in room temperature fluorescence decay measurements with higher time resolution (Du et al., 1992; Muller et al., 1992; Hamm et al., 1993) and play a substantial role in the decay of the stimulated emission from P* at low temperatures [see the accompanying paper (Woodbury et al., 1994)].

Though the fluorescence on the 10-ns time scale has been convincingly identified as arising from the thermal repopu-

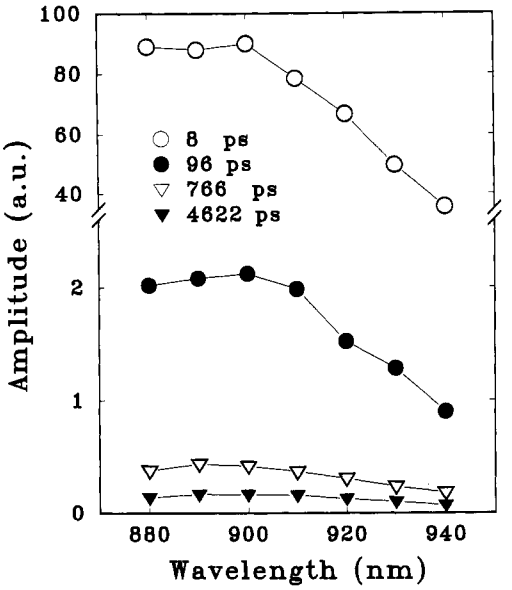

FIGURE 2: Amplitude spectra resulting from global exponential decay analysis of 295 K R-26 reaction center fluorescence at seven wavelengths (880, 890, 900, 910, 920, 930, and 940 nm). Fluorescence decay curves were fit at all wavelengths simultaneously according to the expression $F(t,\lambda) = \sum_i A_i(\lambda)e^{-t/\tau_i}$. Here $F(t,\lambda)$ is the fluorescence as a function of time and wavelength, τ_i are the exponential time constants in the fit, and $A_i(\lambda)$ are the preexponential amplitudes associated with the time constant. The fitting was global; i.e., the time constants were required to be the same at all wavelengths, and the preexponential amplitudes were allowed to vary freely. The figure shows plots of $A_i(\lambda)$ for each τ_i. Note that the scale on the vertical axis is broken and the scale on the lower portion is expanded compared to that on the upper portion.

lation of P* from the long-lived $P^+H_A^-$ state (Woodbury & Parson, 1984; Horber et al., 1986), the subnanosecond delayed fluorescence has not. The multiexponential character of the delayed fluorescence and its persistence at low temperatures could be due to the presence of impurities such as solubilized bacteriochlorophyll or antenna complexes. A number of different experiments were performed in order to rule out this possibility. First, several different reaction center preparations have been used, some involving multiple ion-exchange chromatography steps and/or FPLC chromatography (see Materials and Methods) to ensure the highest possible purity. No significant preparation dependence of the fluorescence decay kinetics or amplitudes was observed. In addition, very similar fluorescence decays are seen in preparations of *Rhodobacter capsulatus* reaction centers (Taguchi et al., 1992).

Plots of the wavelength dependence of the preexponential amplitudes derived from global fitting of decays at seven different wavelengths also support the notion that the different fluorescence decay components all originate from P* (Figure 2). Each of the decay components of the fluorescence has essentially the same spectrum. Similar amplitude spectra have been reported by Holzwarth and co-workers for the 10- and 100-ps decay components (Muller et al., 1992).

It is also possible that some of the shorter components of the delayed fluorescence represent a functional heterogeneity in the reaction center, either because some of the reaction centers are unable to perform electron transfer, giving rise to a long decay time for P*, or because the decay of $P^+H_A^-$ is itself heterogeneous. Previous measurements of the transient absorption changes associated with $P^+H_A^-$ argue against the latter possibility; the decay of this state appears to be nearly single exponential (Schenck et al., 1982; Chidsey et al., 1984). Previous estimates of the P* decay time in the absence of electron transfer and measurement of P* decay in mutants which do not undergo electron transfer place the intrinsic lifetime of P* in the 100–300-ps time range (Breton et al., 1990; Taguchi et al., 1992; Kirmaier & Holten, 1993). Thus, a small population of reaction centers that are incapable of electron transfer could account for some of the observed fluorescence on this time scale. In order to test this possibility and further rule out the involvement of fluorescing contaminants in the sample, reaction centers with quinones in the unreduced state were subjected to actinic illumination, which converted them entirely to the state P^+Q^-. No fluorescence on any time scale was observed when reaction centers were excited at 860 nm under these conditions either at 295 K or at 20 K. From these experiments one can conclude that all fluorescence originates from reaction centers capable of undergoing electron transfer to the quinone, and that there is no detectable fluorescence on any time scale due to either fluorescing contaminants or reaction centers incapable of electron transfer.

Table 3: Comparison of P/P^+ Midpoint Potentials and $P^*/P^+H_A^-$ Standard Free Energy Gaps

sample	P/P^+ [a] (mV)	$\Delta P/P^+$ [b] (cm^{-1})	$\Delta G°$(60 ps) [c] (cm^{-1})	$\Delta\Delta G°$(60 ps) [d] (cm^{-1})
295 K				
R-26	495	0	−1100	0
LH(L131)	575	645	−700	400
double	635	1130	−200	900
20 K				
R-26			−55	0
LH(L131)			−45	10
double			0	55

[a] Data taken from Williams et al. (1992a,b). [b] Change in the P/P^+ midpoint potential between the mutant and R-26 reaction centers. [c] Standard free energy difference at 60 ps between P* and $P^+H_A^-$. 295 K data taken from Figure 5A; 20 K data taken from Figure 5B. [d] Change in the $P^*/P^+H_A^-$ standard free energy gaps at 60 ps between the high-potential mutants and R-26 reaction centers calculated from the standard free energy gaps quoted in the adjacent column.

Fluorescence Decay from High-Potential Mutant Reaction Centers. If all of the delayed fluorescence components are due to thermodynamic repopulation of P* from $P^+H_A^-$, then the amount of delayed fluorescence should be sensitive to the free energy difference between the two states as well as to the P/P^+ midpoint potential. A series of site-directed mutants has been constructed in which the P/P^+ redox potential varies from 415 to about 635 mV (wild type is 495 mV) (Table 3; Williams et al., 1992a,b; Murchison et al., 1993). Relative to wild-type *Rb. sphaeroides*, each mutant reaction center has gained or lost one or more histidine residues capable of forming a hydrogen bond either to one of the ring I acetyl groups or one of the ring V keto groups of P. Panels B and C of Figure 1 show the fluorescence decays of two such mutants, LH(L131) and the double mutant [LH(L131) + LH(M160)], at three temperatures. The amplitudes and kinetic decay constants obtained by fitting the fluorescence decays from these mutants are given in Table 1. The preexponential amplitude spectra for LH(L131) and double-mutant reaction centers at 295 and 20 K show that all of the fluorescence decay components have the same spectrum (data not shown) as was seen in Figure 2 for R-26 reaction centers at 295 K. The amplitudes of the long-lived fluorescence components (A_2 through A_4) increase in the high-potential mutants relative to R-26 reaction centers at all temperatures. It is clear that there is a correlation between the redox potential of P and the amplitude of the delayed fluorescence; a more

positive potential results in larger long-lived fluorescence amplitudes as would be expected if this fluorescence results from the thermal repopulation of P* from $P^+H_A^-$. Table 2 lists the fit to the decay of the fluorescence from the two mutant reaction centers taken over a longer time scale. As was seen for R-26 reaction centers, the lifetimes of the decay components increase when the fluorescence is measured and analyzed on the 16-ns time scale compared to the 8-ns time scale. In order to adequately fit the double-mutant data over a 16-ns time range, or over an 8-ns time range at 20 K, five kinetic components were needed. The fluorescence decay of the double mutant at other temperatures on the 8-ns time scale could also be fit with five components, but the improvement in the quality of the fit was insignificant. The presence of a several-picosecond exponential decay time at 20 K is consistent with the results of transient absorption measurements performed at this temperature [see the accompanying paper (Woodbury et al., 1994)], though it should be noted that the time resolution of the single-photon counting data only allows resolution of components roughly 10 ps or longer, meaning that the exact lifetime reported for the several-picosecond component in Table 1 has a large uncertainty (it could be as long as 10 ps).

DISCUSSION

Work by a number of laboratories has demonstrated that the decay of the excited singlet state in reaction centers from photosynthetic bacteria is complex and requires many exponential decay terms for an adequate description. Decay components of the spontaneous emission have been detected on the 2–3-ps time scale, the 10-ps time scale, the 100-ps time scale, and, in reaction centers with quinones reduced or removed, the 500–1000-ps time scale, the 3–5-ns time scale, and the 10–15-ns time scale (Schenck et al., 1982; Sebban & Moya, 1983; Woodbury & Parson, 1984; Ogrodnik et al., 1988; Williams et al., 1992a; Du et al., 1992; Muller et al., 1992; Hamm et al., 1993).

In the present work, the long-lived fluorescence has been reexamined in detail in the time range from tens of picoseconds to nanoseconds and between the temperatures of 20 and 295 K. In addition, two mutants which increase the midpoint potential of the special pair have been examined. The most significant result of this work is that even at low temperatures (20 K), where an enthalpy gap between P* and $P^+H_A^-$ of more than 100 cm^{-1} would be expected to make detectable thermal repopulation of the excited state impossible, a substantial amount of long-lived fluorescence with the same fluorescence spectrum as P* is observed. This is particularly evident in the mutants in which the P/P^+ midpoint potential is increased, causing the free energy of $P^+H_A^-$ to be closer to that of P*. In the discussion that follows, the issue of whether the long-lived fluorescence is really due to thermal repopulation of P* will be considered first; then, on the basis of the assumption that thermal repopulation does give rise to the long-lived fluorescence, calculations of the time-dependent free energy gap between P* and $P^+H_A^-$ will be performed and discussed in terms of a dynamic solvation model.

The Long-Lived Fluorescence Is Not Due to Contamination or Inactive Reaction Centers. One of the simplest ways to explain the complex fluorescence decay observed in the experiments reported above would be to suppose that the sample is contaminated by small amounts of free pigment or by inactive reaction centers. Particularly in wild-type or R-26 reaction centers, the amplitude of most of the long-lived fluorescence components is small (a few percent or less) as can be seen in Tables 1 and 2. The first argument against contamination is that all of the fluorescence observed in these measurements has essentially the same fluorescence spectrum (Figure 2; Woodbury & Parson, 1984; Muller et al., 1992). However, the strongest evidence against both contaminating pigments and inactive reaction centers is that *all* of the fluorescence using 860-nm excitation disappears upon photoconversion of reaction centers with unreduced quinones to the state $P^+Q_B^-$ (or $P^+Q_A^-$ at low temperature). Reaction centers in the state P^+Q^- neither absorb significantly at 860 nm nor fluoresce significantly near 900 nm when excited at 860 nm. The fluorescence from any free pigment or from reaction centers incapable of undergoing electron transfer would be unchanged by photoconversion. Since no fluorescence was observed under these conditions, all of the fluorescence observed in the quinone-reduced reaction centers must arise from reaction centers capable of undergoing charge separation with reasonable yield.

The Complex P Decay Is Not Entirely the Result of a Static Distribution of Reaction Centers with Different Forward Electron-Transfer Rates.* An alternative explanation of the observed long-lived fluorescence is the presence of several reaction center conformations or distinct populations with different forward electron-transfer rates. As long as these slow reaction centers are able to form $P^+Q_A^-$ with reasonable yield, then fluorescence from these reaction centers would disappear upon steady-state illumination. Though this is a possibility for fluorescence components shorter than about 200 ps, there are several observations and arguments which imply that the longer fluorescence components do not arise in this way.

As argued previously, the longest exponential time constant resulting from fits of the fluorescence decay on a 40-ns time scale has been shown to have a lifetime of the same value and with the same temperature and magnetic field dependence as that observed for the decay of the absorption changes associated with $P^+H_A^-$ in quinone-reduced reaction centers (Woodbury & Parson, 1984; Schenck et al., 1982). For this reason it was concluded that the source of the longest fluorescence component was thermal repopulation of the excited singlet state due to back electron transfer from the state $P^+H_A^-$.

Whether or not the fluorescence decay components in the 100 ps to several nanosecond time range could be explained by subpopulations of reaction centers that undergo electron transfer very slowly depends on what estimate is used for the intrinsic lifetime of P*. Most estimates of the intrinsic lifetime of P* have given numbers in the 100–300-ps range (Holten et al., 1978; Taguchi et al., 1992; Kirmaier & Holten, 1993; Breton et al., 1990). A subnanosecond intrinsic lifetime of the excited singlet state is also consistent with model studies of porphyrin dimers [e.g., Bilsel et al. (1990) and Fujita et al. (1982)]. If these estimates are accurate, then any fluorescence components longer than a few hundred picoseconds in R-26 reaction centers could not be due to slow forward electron transfer. However, since electron transfer in wild-type reaction centers at moderate ambient redox potential and under low excitation light conditions occurs with a yield near 100% (Wraight & Clayton, 1973), the estimates of the intrinsic decay time of P* cited above are based on kinetic studies of reaction centers that have been either mutated or put under conditions where electron transfer to H_A occurs with a decreased yield. It is not clear that these values accurately reflect the intrinsic lifetime of P* in wild-type or R-26 reaction centers. In fact, there has been one report of

a mutant with an intrinsic lifetime of P* longer than 300 ps at 295 K (Nagarajan et al., 1990).

In the high-potential mutants, particularly LH(L131), the situation is clearer in this regard. The yield of initial charge separation in LH(L131) has been previously determined to be about 70% at room temperature, and the bulk of the electron transfer occurs with a time constant between 13 and 21 ps at this temperature (Williams et al., 1992a). This implies that the pathway competing with the forward electron-transfer reaction has a time constant of less than 100 ps (discussed in detail below). Yet in this mutant, the long-lived fluorescence components have lifetimes of roughly 120 ps, 800 ps, and several nanoseconds at room temperature (Table 1). The same can be said of at least two other high-potential mutants for which careful fluorescence decay measurements have been performed. Both *sym1*, a *Rb. capsulatus* symmetry mutation (Taguchi et al., 1992; Stocker et al., 1992), and LH(M160), another hydrogen bond mutant in *Rb. sphaeroides* (Williams et al., 1992a), have decreased yields of electron transfer at room temperature which give rise to estimates of intrinsic excited-state decay times of less than 100 ps. Yet both of these mutants, like LH(L131), have fluorescence components on the 100-ps, 800-ps, and several-nanosecond time scales, arguing strongly that these components are not due to a decrease in the electron-transfer rate from P* to $P^+H_A^-$ in some subpopulation of the reaction centers.

In addition to the experimental findings and arguments presented above, there are other reasons to believe that the long-lived fluorescence components do not arise from artificially slow reaction centers that have been damaged during preparation. Very similar decay components are observed in whole photosynthetic membranes (Woodbury & Parson, 1986) as well as in the fluorescence from other photosystems that are evolutionarily very distant such as photosystem II (Booth et al., 1991), photosystem I, and the *Heliobacillus mobilis* photosystem (Kleinherenbrink et al., 1994). In these evolutionarily very diverse systems the same basic pattern of fluorescence decay is observed. In photosystem II reaction centers, where measurements have been performed over a broad range of temperatures, the same unusual temperature dependence of the long-lived fluorescence is observed. In fact, in each of these systems, a remarkable similarity is found not only in the kinetic behavior of the long-lived fluorescence but in its relative amplitude. Therefore, the predicted free energy gaps between the charge-separated and excited states in these different systems are quite similar as well. This suggests that the complex decay of P* is not the result of some peculiar trait of purple bacterial reaction centers or of the procedures used to isolate them.

Dynamic Solvation of the Charge-Separated State. Another possible explanation of the complex time and temperature dependence of the fluorescence is that a time-dependent solvation of the charge-separated state takes place during the picoseconds and nanoseconds which follow the initial electron-transfer reaction. In the simplest form of this model, all the fluorescence arises from a single population of reaction centers but the large number of degrees of freedom inherent in the protein results in solvation of the charge-separated state, which proceeds on many time scales. If P* is energetically close enough to $P^+H_A^-$ for thermal repopulation to occur, then the P* decay kinetics would become complex due to the changing amount of thermal repopulation of P* as solvation of the charge-separated state progresses. Solvation results in a time-dependent increase in the magnitude of the free energy gap between P* and $P^+H_A^-$. Similar models have been proposed previously to explain the fluorescence from P* on the nanosecond time scale (Woodbury & Parson, 1984) and to explain the yield and decay of ^3P (Goldstein & Boxer, 1989).

Temperature Dependence of the Long-Lived Fluorescence. One of the most successful applications of the dynamic solvation model is in explaining the complex temperature dependence of the long-lived fluorescence amplitudes. If only a single form of the charge-separated state were present at all times, one would expect that the thermal repopulation of P* from $P^+H_A^-$ would decrease dramatically as the temperature was lowered, resulting in a concomitant decrease in the fluorescence amplitude. In fact, the amplitude of the longest-lived fluorescence component increases as the temperature decreases from 270 to 200 K (Woodbury & Parson, 1984; this increase can also be seen in Table 1 by comparing the 295 and 100 K data), and the amplitudes of the subnanosecond components never decrease. In the solvation model, this increase in fluorescence amplitude with decreasing temperature occurs because some of the solvation processes slow down or cease to occur as the temperature is lowered, which forces $P^+H_A^-$ to remain energetically closer to P* over the time scale of the measurement. The entire complex temperature dependence of the long-lived fluorescence can be understood in terms of two competing processes: (1) the freezing out of motion involved in solvation, which tends to increase the amount of fluorescence due to thermal repopulation by forcing $P^+H_A^-$ to remain closer to P* in energy, and (2) the tendency for the thermal repopulation of P* to decrease with decreasing temperature as k_BT becomes smaller relative to the enthalpy gap between P* and $P^+H_A^-$.

A time- and temperature-dependent enthalpy gap between P* and $P^+H_A^-$ also explains the apparent discrepancy between the fast time scale estimates of the free energy gap as studied by fluorescence decay measurements (this work; Woodbury & Parson, 1984; Schenck et al., 1982) and the slower time scale estimates of the free energy gap between P* and $P^+H_A^-$ from the triplet yield and decay (Goldstein et al., 1988; Ogrodnik et al., 1988). As solvation occurs, there is a time-dependent increase in the enthalpy between the excited and charge-separated states. Thus, on the long time scale of the ^3P measurements, the free energy gap is much larger than on the short time scale of the fluorescence measurements. One would also expect that on the time scale of ^3P decay (microseconds) there would be less temperature dependence to the free energy gap between P* and $P^+H_A^-$, as is observed, since, given microseconds, many of the solvation processes which slow down as the temperature is lowered will still go to completion.

Calculation of the Time-Dependent Concentrations of P and $P^+H_A^-$ Using the Solvation Model.* The remainder of the discussion will explore the ramifications of the dynamic solvation model. Specifically, the time-dependent populations of P*, $P^+H_A^-$, and P will be determined using a simple, sequential kinetic model, and the standard free energy gap between P* and $P^+H_A^-$ will be evaluated as a function of time. Unlike previous estimates of the driving force for initial electron transfer based on the relative amplitudes of preexponential terms derived from fits such as those described in Table 1 (Schenck et al., 1982; Woodbury & Parson, 1984; Taguchi et al., 1992; Williams et al., 1992a), the calculations which follow use the fits only as an accurate representation of the data in which the instrument response function has been removed. This is important, since the relative preexponential amplitudes associated with each decay term, and thus the results of an analysis based on the values of these fitting

Scheme 2

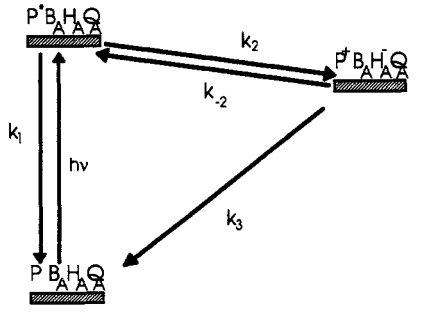

parameters, can vary with the time scale over which the analysis is performed (e.g., compare the fit for the double mutant at 295 K between Tables 1 and 2). Below, the instantaneous populations of P*, $P^+H_A^-$, and the ground state as a function of time are calculated directly from the time course of the fluorescence (as accurately represented by the fit), and this is used to determine the time-dependent $P^*/P^+H_A^-$ free energy gap.

Upon charge separation, the protein will begin to reorganize around the newly formed anion and cation, resulting in a decrease in the standard free energy of the state $P^+H_A^-$. The dynamic solvation of $P^+H_A^-$ will lead to an increase in the free energy gap between P* and $P^+H_A^-$ and consequently an increase in the equilibrium constant $K_{eq} = k_2/k_{-2} = [P^+H_A^-]/[P^*]$ (Scheme 2). If one assumes that charge separation is fast on the time scale of these measurements, then the populations of P* and $P^+H_A^-$ should remain close to their equilibrium values. Given that the amount of fluorescence at any time is proportional to the concentration of P*, then knowledge of $[P^+H_A^-]$ would be sufficient information to calculate the standard free energy gap between P* and $P^+H_A^-$ without knowledge of forward or backward rate constants of electron transfer. If P* and $P^+H_A^-$ are the only states important for describing electron transfer on the time scale of these measurements [a topic which is addressed in detail in the accompanying paper (Woodbury et al., 1994)], then Scheme 2 represents a simplification of Scheme 1 consistent with the time resolution and range of the fluorescence data in Table 1.

Equations 1–4 are the differential equations which determine the time dependence of population of the individual states.

$$d[P^*]/dt = -(k_1 + k_2)[P^*] + k_{-2}[P^+H_A^-] \quad (1)$$

$$d[P^+H_A^-]/dt = k_2[P^*] - (k_{-2} + k_3)[P^+H_A^-] \quad (2)$$

$$[P](t) = [P^*](0) - [P^*](t) - [P^+H_A^-](t) \quad (3)$$

$$[P^*](0) = 1 \quad (4)$$

Using the time-dependent fluorescence intensity (as represented by the exponential decay components resulting from the fits described in Table 1) to determine the population of P* as a function of time, an iterative application of eqs 1–4 will yield the time dependence of $[P^+H_A^-]$ and the ground-state [P].

In order to perform these calculations, there are three parameters which must be specified that are not determined in the experiments described in this work: the decay time of $P^+H_A^-$ when electron transfer to the quinone is blocked ($1/k_3$), the intrinsic decay time of P* in the absence of electron transfer ($1/k_1$), and the initial amplitude of the fluorescence at zero time (which is not resolved in these measurements due to limited time resolution).

The decay time of $P^+H_A^-$ ($1/k_3$) has been measured in R-26 reaction centers with reduced quinones and has been found to be about 10 ns (Schenck et al., 1982). As long as this decay time is still on the nanosecond time scale in the mutants (and the lifetime of the longest-lived component of the fluorescence in each case is consistent with this assumption), the exact value used for this parameter will have little effect on the free energy calculations during the first few nanoseconds. Thus, 10 ns was used for the analysis of the fluorescence decays from all samples.

In samples where the yield of electron transfer is high, the intrinsic decay rate of P* ($1/k_1$) does not have a very great effect on the kinetics of P* decay. However, in the LH(L131) mutant, as well as in the double mutant at low temperature, there is some ground-state recovery during the initial electron-transfer reaction, at least at certain temperatures (Williams et al., 1992a; Woodbury et al., 1994), and therefore this decay path has been included, even though its effect on the free energies calculated during the first few nanoseconds is small. Interestingly, the inclusion of an intrinsic P* decay rate has more effect on the free energy calculations at long times (3 ns and longer) due to the fact that some of the charge-separated state decays back through P* to the ground state, particularly in the high-potential mutants.

There is no way of directly measuring the intrinsic rate constant of P* decay (k_1) in reaction centers that undergo electron transfer with 100% yield. However, a measurement of P* decay has been made in a mutant of *Rb. capsulatus* in which H_A is apparently lost (Vos et al., 1991). The value reported there is 190 ps, and we have used this in the calculations below for the R-26 reaction center data. In reaction centers from LH(L131) (Williams et al., 1992a,b), the decreased yield of electron transfer ($\phi_{et} = 70 \pm 10\%$) and the decreased overall rate of P* decay or ground-state recovery (this is wavelength dependent, but $\tau_{obs} = 21$ ps at 850 nm) allows one to estimate the intrinsic decay time of P* as $k_1 = (1 - \phi_{et})/\tau_{obs}$, where ϕ_{et} is the quantum yield of charge separation for electron transfer to H_A, and τ_{obs} is the observed time constant of P* decay or ground-state recovery, resulting in a value of $(75 \pm 25 \text{ ps})^{-1}$ for k_1. For standard free energy calculations on the double-mutant sample, an intrinsic P* decay rate of $(300 \text{ ps})^{-1}$ was used, estimated from the yield and the overall P* decay rate at 20 K (Woodbury et al., 1994).

Though there is some uncertainty in the values of k_1 and k_3 used, the free energy calculations described below depend logarithmically on the relative P* and $P^+H_A^-$ concentrations, so the results are only weakly dependent on the exact values of either k_1 or k_3. This is particularly true in R-26 reaction centers, since the overall decay rate of P* is nearly 100-fold faster than k_1, and k_3 has been directly measured (Schenck et al., 1982). The calculations below were also performed using $k_1 = k_3 = 0$, and this had very little effect on the values reported for the free energy difference between P* and $P^+H_A^-$, particularly on time scales shorter than 1 ns.

Finally, because the initial decay of the excited state is sometimes faster than the time resolution of the single-photon counting apparatus used (this is true at least in R-26 reaction centers), the amplitude of the fluorescence at zero time cannot always be accurately determined from these data alone. In principle, the initial amplitude of the fluorescence can be determined from the exponential fit and deconvolution as $A_1 + A_2 + A_3 + A_4$. The difficulty is in determining the correct value of A_1 when the initial fluorescence decay is faster than

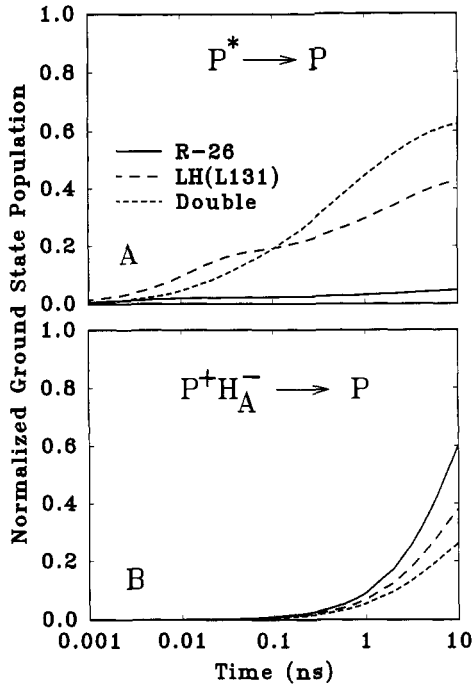

FIGURE 3: Time-dependent relative populations of P* and $P^+H_A^-$ for R-26, LH(L131), and double-mutant reaction centers calculated using eqs 1–4 and the exponential fits of the fluorescence decays at 295 K. Assuming an initial population of P* normalized to 1.0, the amount of P* decay at each time point was determined from the fits of the fluorescence decay curves (performed as in the caption to Figure 2), and then, given the values of k_1 and k_3 described in the text, the amount of $P^+H_A^-$ formed and the amount of ground state recovered at each step was calculated. Time is plotted on a logarithmic scale.

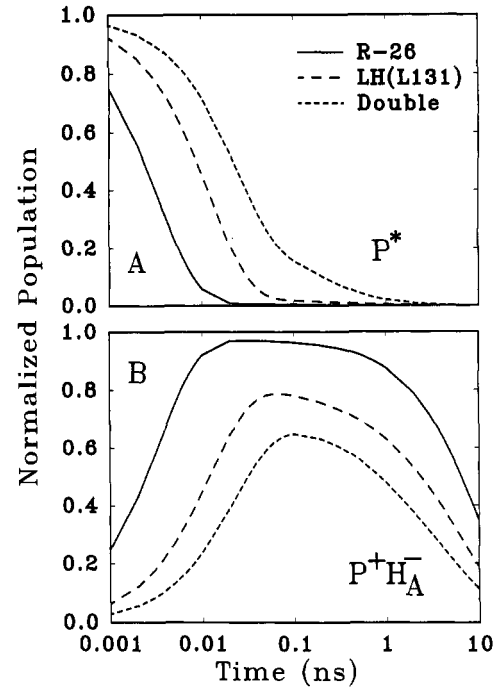

FIGURE 4: Fraction of ground state recovered as a function of time at 295 K for R-26, LH(L131), and double-mutant reaction centers. As in Figure 3, the initial excited-state population is normalized to 1.0. (A) Ground-state recovery due to decay of the excited singlet state to the ground state. This corresponds to all ground-state recovery that occurs via the path with the rate constant k_1 in Scheme 2. (B) Ground-state recovery due to recombination in the state $P^+H_A^-$. This corresponds to all ground-state recovery that occurs via the path with the rate constant k_3 in Scheme 2. The population of the ground state generated via each path is determined using the same equations and methods described in the caption to Figure 3. Time is plotted on a logarithmic scale.

the instrument's time resolution. In order to overcome this limitation, A_1 was corrected, as described previously (Taguchi et al., 1992). $A_1(\text{corrected}) = A_1(\text{obs})\tau_1/\tau_{obs}$, where τ_{obs} is determined through high-resolution femtosecond experiments. Measurements of τ_{obs} by femtosecond transient optical spectroscopy have been performed at several temperatures between 295 and 20 K for R-26 and LH(L131) reaction centers, and intermediate values have been extrapolated from these measurements (R. G. Alden, J. M. Peloquin, J. C. Williams, J. P. Allen, and N. W. Woodbury, unpublished results; see caption to Figure 6). For the double mutant, the corrections were performed at 295 and 20 K where reliable τ_{obs} values were available (Williams et al., 1992b; Woodbury et al., 1994), though these corrections had little effect on the free energy gap determined. At intermediate temperatures in the double mutant, the fluorescence data were analyzed without correction.

Figure 3 shows the calculated time dependence of the populations of P* and $P^+H_A^-$ for reaction centers from R-26, LH(L131), and the double mutant. The differences in the P* decays in Figure 3A are primarily due to the decrease in the initial rate of electron transfer in LH(L131) and the double mutant relative to R-26 reaction centers. Figure 3B shows the appearance of the charge-separated state as P* decays in each case. On longer time scales, charge recombination in $P^+H_A^-$ dominates, and the population of the charge-separated state decreases.

There are two decay pathways to the ground state at any time, one from $P^+H_A^-$ (charge recombination, k_3 in Scheme 2) and one directly from P* (k_1 in Scheme 2). Figure 4A shows the amount of ground-state recovery through P*. In R-26 reaction centers this is the dominant pathway for ground-state recovery only during the first nanosecond. After 1 ns, ground-state recovery predominantly occurs via charge recombination of $P^+H_A^-$ for R-26 as shown in Figure 4B. In LH(L131) and double-mutant reaction centers, ground-state recovery at all times proceeds primarily via P*. This is because in the high-potential mutants, the activation energy for decay of $P^+H_A^-$ via P* is small. Similar results have been observed previously for reaction centers from the high-potential mutant *syml* (Taguchi et al., 1992).

$P^*/P^+H_A^-$ Free Energy Difference vs Time at Room Temperature. Figure 5A is a plot of the free energy difference between P* and $P^+H_A^-$ at 295 K calculated from the populations in Figure 3 using eqs 5 and 6 and assuming thermal equilibrium between P* and $P^+H_A^-$.

$$K_{eq}(t) = [P^+H_A^-](t)/[P^*](t) \quad (5)$$

$$\Delta G^\circ(t) = -RT \ln K_{eq}(t) \quad (6)$$

The rate of approach to equilibrium between P* and $P^+H_A^-$ is given by the sum of the forward and backward rate constants for the initial electron transfer. For R-26 reaction centers, which undergo the bulk of P* decay on the few-picosecond time scale, thermal equilibration between P* and $P^+H_A^-$ should be achieved within 10 ps. LH(L131) shows a slower decay of the stimulated emission at room temperature (about 13 ps). If this decay time represents the rate of electron transfer, then one would expect that thermal equilibration in this mutant would take place after about 30 ps. In the double mutant, which undergoes the bulk of its P* decay on the 20-ps time scale at room temperature, thermal equilibration should be nearly complete in about 60 ps. In Figure 5, free energy

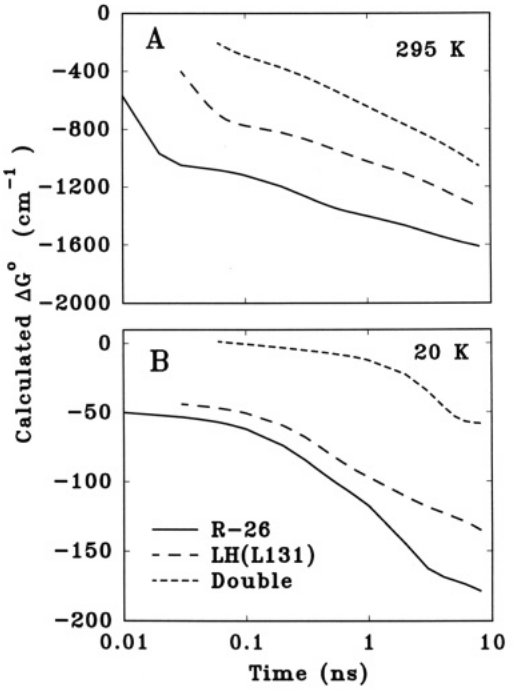

FIGURE 5: Time-dependent standard free energy difference between P* and $P^+H_A^-$ calculated as $-RT\ln([P^*]/[P^+H_A^-])$ assuming thermal equilibrium between the two states. The time-dependent populations of P* and $P^+H_A^-$ were calculated as in the caption to Figure 3. (A) Results of the calculations at 295 K using values for the rate constants k_1 and k_3 as follows: k_1(R-26) = 1/(190 ps); k_1(LH(L131)) = 1/(75 ps); k_1(double mutant) = 1/(300 ps); k_3 = 1/(10 000 ps) for all samples. (B) Results of the calculations at 20 K using k_1(R-26) = 1/(190 ps), k_1(LH(L131)) = 1/(75 ps), k_1(double mutant) = 1/(300 ps), and k_3 = 1/(10 000 ps) for all samples. Time is plotted on a logarithmic scale.

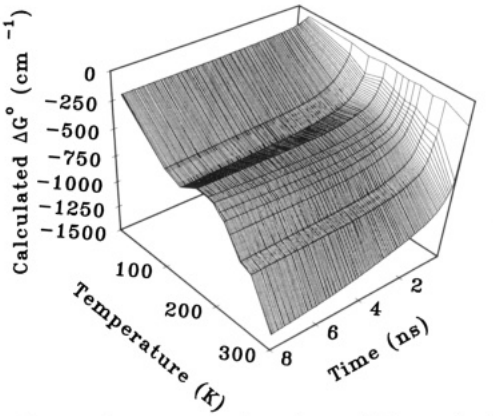

FIGURE 6: Time and temperature dependence of the standard free energy difference between P* and $P^+H_A^-$ for LH(L131) reaction centers. The free energy gap was calculated as in Figure 5 using k_1 = 1/(75 ps) and k_3 = 1/(10 000 ps) for all temperatures. The P* decay values used to correct the amplitude of the prompt fluorescence, A_1 (see text), were measured by subpicosecond-resolution transient absorption spectroscopy (R. G. Alden, J. M. Peloquin, J. C. Williams, J. P. Allen, and N. W. Woodbury, unpublished) as 12.2 ps for 295 K, 10.6 ps for 100 K, and 3.7 ps for 20 K. Decay times at intermediate temperatures were estimated by linear interpolation.

calculations are shown only from the expected time of equilibration onward. Each of the three reaction centers displays an increase in the magnitude of the calculated standard free energy difference between P* and $P^+H_A^-$ with increasing time. Such an increase is consistent with the proposed solvation of the charge-separated state by the protein. The change in the free energy difference with time is particularly steep during the first 100 ps. This may have physiological significance since *in vivo* (or in unreduced reaction centers) $P^+H_A^-$ only lives for about 200 ps (Kirmaier & Holten, 1987). At 8 ns, the $P^*/P^+H_A^-$ standard free energy gap for R-26 reaction centers is -1600 cm^{-1} in Figure 5A, which is about 70% of the value predicted from studies of the ^{3}P state (Goldstein et al., 1988). Allowing for further relaxation around the charge-separated state on longer time scales, these results seem consistent with those obtained from ^{3}P decay and yield measurements, at least at room temperature.

Temperature Dependence of the $P^*/P^+H_A^-$ Standard Free Energy Gap. The most striking aspect of this study is the persistence of the long-lived fluorescence at 20 K (Figure 1; Table 1). If one assumed that the 295 K standard free energy difference at 1 ns in Figure 5A (about -1400 cm^{-1}) was temperature independent, then the amount of fluorescence at 1 ns should decrease by a factor of more than 10^{40} when the temperature is dropped to 20 K. Even in LH(L131) and the double mutant, which have nanosecond free energy gaps of roughly -1000 and -800 cm^{-1}, respectively, at room temperature (Figure 5A), one would not expect to observe any long-lived fluorescence at low temperature if these free energy gaps remained constant. However, there is clearly substantial long-lived fluorescence present on the nanosecond time scale, particularly in reaction centers from the high-potential mutants (Figure 1).

Figure 5B shows the $P^*/P^+H_A^-$ free energy difference calculated for the three reaction centers as a function of time at 20 K. Consistent with previous work (Woodbury & Parson, 1984), the calculated free energy difference between P* and $P^+H_A^-$ is markedly reduced at low temperatures in all samples. In terms of time-dependent solvation of the charge-separated state, the decrease in the $P^*/P^+H_A^-$ standard free energy gap with decreasing temperature would be explained as a slowing down or freezing out of the protein motions which stabilize the charge-separated state and thus increase the free energy gap between P* and $P^+H_A^-$. Some reorganization of the protein around $P^+H_A^-$ apparently still takes place even at 20 K since all three reaction centers show a time-dependent increase in the $P^*/P^+H_A^-$ free energy gap over the time scale of the experiment (Figure 5B).

The time and temperature dependence of $\Delta G°$ indicate a solvation-dependent enthalpy. It has previously been suggested that the calculated decrease in the $P^*/P^+H_A^-$ free energy gap with decreasing temperature indicated that a large fraction of the free energy difference was entropic (Woodbury & Parson, 1984). Such an interpretation is at odds with the nearly temperature independent free energy difference which was calculated from studies of the ^{3}P state (Goldstein et al., 1988; Ogrodnik et al., 1988; Takiff & Boxer, 1988). Figure 6 shows the calculated free energy surface as a function of both time and temperature for LH(L131) reaction centers. This figure reemphasizes the fact that the relative $P^*/P^+H_A^-$ free energy gap decreases dramatically as one goes to shorter times and lower temperatures. This is more consistent with a time- and temperature-dependent enthalpy than with a purely entropic $P^*/P^+H_A^-$ free energy gap. If solvation of the charge-separated state involves motion on the nanosecond time scale, one would expect that at early times, before the solvation has had a chance to occur, or at low temperature, when many motions are slowed down or frozen out, $P^+H_A^-$ would be in a less relaxed state relative to P*.

The Calculated $P^*/P^+H_A^-$ Free Energy Gap at Early Times and/or Low Temperatures Is Surprisingly Small. The results of the standard free energy gap calculations in Figures 5 and 6 indicate that the driving force for electron transfer on the

tens of picoseconds time scale is only a few hundred wavenumbers for R-26 reaction centers at room temperature and less for the two mutants. At low temperature, the values drop to the tens of wavenumbers scale. Though one might expect that the free energy stabilization of the charge-separated state due to dynamic solvation would go essentially to zero at early times and low temperatures, one would still expect there to be some very fast, essentially temperature independent internal reorganization energy associated with electron transfer which would be larger than a few hundred wavenumbers [discussed in the accompanying paper (Woodbury et al., 1994)].

It is possible that thermal repopulation does not account for all of the complexity in the P* decay at early times. One could explain the early time fluorescence decay complexity in terms of a static distribution of reaction centers. Indeed, the conformational changes proposed above to give rise to dynamic solvation of the charge-separated state would be expected to give rise to a distribution of $P^+H_A^-$ and/or P* energies within the reaction center population at any given time. This distribution itself may account for some of the complexity of the fluorescence decay, particularly on early time scales and at low temperatures where one would expect that such a distribution would be essentially static [see the accompanying paper (Woodbury et al., 1994)]. However, a static distribution of reaction centers cannot explain the fluorescence decay kinetics on time scales longer than the intrinsic lifetime of the excited state (75–200 ps depending on the reaction center sample; see above). Thus, at least on time scales of hundreds of picoseconds or longer, the primary source of fluorescence is thermal repopulation of P*. This can only be true if the $P^*/P^+H_A^-$ free energy gap is very small, as described above, particularly at low temperature.

Effect of Changing the P/P⁺ Midpoint Potential on the P/P⁺H$_A^-$ Free Energy Gap.* Table 3 compares the P/P^+ midpoint potentials of R-26 reaction centers and the two mutant reaction centers with the $P^*/P^+H_A^-$ standard free energy difference at 60 ps, a time when all three reaction centers should have achieved thermal equilibration, at both 295 and 20 K. At room temperature, one sees a discrepancy between the increase in the steady-state redox potentials for the mutants and the changes in the relative free energies of $P^+H_A^-$ determined from the fluorescence. Between R-26 and LH(L131), the P/P^+ midpoint potential increased by 80 mV (645 cm^{-1}). One would estimate that this would result in a 645 cm^{-1} decrease in the standard free energy gap between P* and $P^+H_A^-$ in this mutant relative to R-26. There is a substantial decrease in the free energy gap, but it only amounts to a change of about 400 cm^{-1}. A similar discrepancy exists between the steady-state redox potential of P and the $P^*/P^+H_A^-$ free energy gap comparing R-26 to the double mutant.

It would probably be possible to explain these discrepancies at room temperature by noting that the free energy of $P^+H_A^-$ depends on both the P/P^+ midpoint potential and the H/H^- reduction potential. It is possible that there is a stabilization of the bacteriopheophytin anion in the mutants which partially offsets the destabilization of P^+. In addition, the steady-state redox titrations were performed at moderate potential where the quinones were not in the reduced state. The presence of the quinone anion in the fluorescence measurements (which were performed under reducing conditions) may also have affected the energy of $P^+H_A^-$ in a way that was dependent on the mutation.

However, these effects do not easily explain the low-temperature results where the differences between the $P^*/P^+H_A^-$ standard free energy gaps of R-26 and the two mutants, like the free energy gaps themselves, are less than 100 cm^{-1}. If the steady-state redox potential changes were due to static coulombic interactions, for example, between the dipole formed by the hydrogen bond and the cation of P, then one would not expect that the energy differences between the mutants would be so temperature dependent. One possible explanation of the discrepancies is that part of the effect of the mutations is to limit the extent of solvation of the charge-separated state. It is possible that the hydrogen bonds between the protein and P that raise the P/P^+ midpoint potential do so because they limit the ability of the local environment to relax around the cation. In this case, one would not expect as much of a difference between R-26 and the two mutant samples at early times or low temperatures (where little solvation has occurred in any case) as would be observed in a steady-state redox titration at room temperature.

As described below and in the accompanying paper (Woodbury et al., 1994), however, there is an alternate explanation both for the apparently small driving forces calculated for R-26 and for the inconsistencies between the measured changes in P/P^+ potentials vs the $P^*/P^+H_A^-$ standard free energies in the mutants. This involves a reexamination of the initial electron-transfer mechanism in light of the results presented above.

Mechanistic Implications. The conclusion that the driving force of initial electron transfer on the picosecond time scale in the reaction center is on the order of tens to hundreds of wavenumbers raises numerous questions about the mechanism of the initial electron transfer. If the free energy change for the reaction is actually smaller than the internal reorganization energy of the system (meaning the reorganization energy due to small nuclear conformational changes of the cofactors involved in the electron-transfer reaction), then one would expect that the rate of electron transfer would decrease significantly with temperature, according to traditional treatments of nonadiabatic electron transfer [e.g., Closs and Miller (1988)]. This is not observed.

If the above analysis is correct, then, at least at low temperature, nonadiabatic electron transfer theory, which assumes weakly coupled excited and charge-separated states, is not an adequate description of the initial electron-transfer mechanism in the reaction center. This is true even in the limit that one only accepts the free energy estimates on the nanosecond time scale, where it is difficult to envision a mechanism other than thermal repopulation of P* to explain the significant fluorescence amplitude. It may be more reasonable to consider the possibility that electron transfer is adiabatic, and that P* and the charge-separated states are strongly coupled (at least for certain nuclear configurations of the system). In this case, a single continuous potential surface exists between the initial excited state and the final charge-separated state. The lack of temperature dependence of the rate comes about because the slope of the potential surface between the reactant and the product is everywhere small or negative due to some combination of strong electronic coupling between P* and $P^+H_A^-$, at least in certain regions of the potential surface, and the inherent shapes of the zero-order potential surfaces of P* and $P^+H_A^-$. These concepts will be developed further in the accompanying paper (Woodbury et al., 1994).

In this view, the rate of the initial reaction is limited by the evolution of the nuclear configuration of the system. What one is observing by monitoring the fluorescence as a function of time is movement of the average nuclear configuration of

the system away from the region of Frank–Condon overlap with the ground state. This is, in effect, the extreme limit of the dynamic solvation concept where the entire reaction is driven and rate limited by changes in the nuclear configuration with time, resulting in a nonexponential decay of the emission extending from picoseconds to nanoseconds.

ACKNOWLEDGMENT

The authors wish to thank Drs. W. Parson, S. Boxer, D. Holten, D. Gust, and T. Moore for many helpful discussions and P. Horton for preparation of reaction centers.

REFERENCES

Allen, J. P., Feher, G., Yeates, T. O., Komiya, H., & Rees, D. C. (1987) *Proc. Natl. Acad. Sci. U.S.A. 84*, 5730–5734.
Bilsel, O., Rodriguez, J., & Holten, D. (1990) *J. Phys. Chem. 94*, 3508–3512.
Booth, P. J., Crystall, B., Ahmad, I., Barber, J., Porter, G., & Klug, D. R. (1991) *Biochemistry 30*, 7573–7586.
Breton, J., Martin, J.-L., Lambry, J.-C., Robles, S. J., & Youvan, D. C. (1990) in *Reaction Centers of Photosynthetic Bacteria* (Michel-Beyerle, M.-E., Ed.) pp 293–302, Springer, Berlin.
Chan, C.-K., DiMagno, T. J., Chen, L. X.-Q., Norris, J. R., & Fleming, G. R. (1991) *Proc. Natl. Acad. Sci. U.S.A. 88*, 11202–11207.
Chang, C.-H., El-Kabbani, O., Tiede, D., Norris, J., & Schiffer, M. (1991) *Biochemistry 30*, 5352–5360.
Chidsey, C. E. D., Kirmaier, C., Holten, D., & Boxer, S. G. (1984) *Biochim. Biophys. Acta 776*, 424–437.
Closs, G. L., & Miller, J. R. (1988) *Science 240*, 440–447.
Deisenhofer, J., Epp, O., Miki, K., Huber, R., & Michel, H. (1984) *J. Mol. Biol. 180*, 385–398.
Du, M., Rosenthal, S. J., Xie, X., DiMagno, T. J., Schmidt, M., Hanson, D. K., Schiffer, M., Norris, J. R., & Fleming, G. R. (1992) *Proc. Natl. Acad. Sci. U.S.A. 89*, 8517–8521.
Feher, G., & Okamura, M. Y. (1978) in *The Photosynthetic Bacteria* (Clayton, R. K., & Sistrom, W. R., Eds.) pp 349–386, Plenum Press, New York.
Feher, G., Allen, J. P., Okamura, M. Y., & Rees, D. C. (1989) *Nature 339*, 111–116.
Fujita, I., Fajer, J., Chang, C.-K., Wang, C.-B., Bergkamp, M. A., & Netzel, T. L. (1982) *J. Phys. Chem. 86*, 3754–3759.
Goldstein, R. A., & Boxer, S. G. (1989) *Biochim. Biophys. Acta 977*, 78–86.
Goldstein, R. A., Takiff, L., & Boxer, S. G. (1988) *Biochim. Biophys. Acta 934*, 253–263.
Gust, D., Moore, T. A., Luttrull, D. K., Seely, G. R., Bittersmann, E., Bensasson, R. V., Rougee, M., Land, E. J., DeSchryver, F. C., & Van der Auweraer, M. (1990) *Photochem. Photobiol. 51*, 419–426.
Hamm, P., Gray, K. A., Oesterhelt, D., Feick, R., Scheer, H., & Zinth, W. (1993) *Biochim. Biophys. Acta 1142*, 99–105.
Holten, D., Windsor, M. W., Parson, W. W., & Thornber, J. P. (1978) *Biochim. Biophys. Acta 501*, 112–126.
Holzapfel, W., Finkele, U., Kaiser, W., Oesterhelt, D., Scheer, H., Stilz, H. U., & Zinth, W. (1989) *Chem. Phys. Lett. 160*, 1–7.
Horber, J. K. H., Gobel, A., Ogrodnik, A., Michel-Beyerle, M. E., & Cogdell, R. J. (1986) *FEBS Lett. 198*, 268–272.
Kirmaier, C., & Holten, D. (1987) *Photosynth. Res. 13*, 225–260.
Kirmaier, C., & Holten, D. (1990) *Proc. Natl. Acad. Sci. U.S.A. 87*, 3552–3556.
Kirmaier, C., & Holten, D. (1993) in *The Photosynthetic Reaction Center, Vol. II* (Norris, J. R., Ed.) pp 49–69, Academic Press, San Diego.
Kirmaier, C., Holten, D., Bylina, E. J., & Youvan, D. C. (1988) *Proc. Natl. Acad. Sci. U.S.A. 85*, 7562–7566.
Kleinherenbrink, F. A. M., Hastings, G., Wittmershaus, B. P., & Blankenship, R. E. (1994) *Biochemistry* (in press).
Martin, J.-L., Breton, J., Hoff, A. J., Migus, A., & Antonetti, A. (1986) *Proc. Natl. Acad. Sci. U.S.A. 83*, 957–961.
Michel-Beyerle, M. E., Plato, M., Deisenhofer, J., Michel, H., Bixon, M., & Jortner, J. (1988) *Biochim. Biophys. Acta 932*, 52–70.
Muller, M. G., Griebenow, K., & Holzwarth, A. R. (1992) *Chem. Phys. Lett. 199*, 465–469.
Murchison, H. A., Alden, R. G., Allen, J. P., Peloquin, J. M., Taguchi, A. K. W., Woodbury, N. W., & Williams, J. C. (1993) *Biochemistry 32*, 3498–3505.
Nagarajan, V., Parson, W. W., Gaul, D., & Schenck, C. C. (1990) *Proc. Natl. Acad. Sci. U.S.A. 87*, 7888–7892.
Ogrodnik, A., Volk, M., Letterer, R., Feick, R., & Michel-Beyerle, M. E. (1988) *Biochim. Biophys. Acta 936*, 361–371.
Parson, W. W. (1991) in *Chlorophylls* (Scheer, H., Ed.) pp 1153–1180, CRC Press, Boca Raton, FL.
Parson, W. W., & Warshel, A. (1987) *J. Am. Chem. Soc. 109*, 6152–6163.
Schenck, C. C., Blankenship, R. E., & Parson, W. W. (1982) *Biochim. Biophys. Acta 680*, 44–59.
Sebban, P., & Moya, I. (1983) *Biochim. Biophys. Acta 722*, 436–442.
Shuvalov, V. A., & Parson, W. W. (1984) *Biochim. Biophys. Acta 638*, 50–59.
Stocker, J. W., Taguchi, A. K. W., Murchison, H. A., Woodbury, N. W., & Boxer, S. G. (1992) *Biochemistry 31*, 10356–10362.
Taguchi, A. K. W., Stocker, J. W., Alden, R. G., Causgrove, T. P., Peloquin, J. M., Boxer, S. G., & Woodbury, N. W. (1992) *Biochemistry 31*, 10345–10355.
Takiff, L., & Boxer, S. G. (1988) *Biochim. Biophys. Acta 932*, 495–510.
Vos, M. H., Lambry, J.-C., Robles, S. J., Youvan, D. C., Breton, J., & Martin, J.-L. (1991) *Proc. Natl. Acad. Sci. U.S.A. 88*, 8885–8889.
Warshel, A., & Parson, W. W. (1987) *J. Am. Chem. Soc. 109*, 6143–6152.
Williams, J. C., Alden, R. G., Murchison, H. A., Peloquin, J. M., Woodbury, N. W., & Allen, J. P. (1992a) *Biochemistry 31*, 11029–11037.
Williams, J. C., Alden, R. G., Coryell, V. H., Lin, X., Murchison, H. A., Peloquin, J. M., Woodbury, N. W., & Allen, J. P. (1992b) in *Research in Photosynthesis* (Murata, N., Ed.) Vol. 1, pp 377–380, Kluwer Academic Publishers, Dordrecht.
Woodbury, N. W., & Parson, W. W. (1984) *Biochim. Biophys. Acta 767*, 345–361.
Woodbury, N. W., & Parson, W. W. (1986) *Biochim. Biophys. Acta 850*, 197–210.
Woodbury, N. W., Becker, M., Middendorf, D., & Parson, W. W. (1985) *Biochemistry 24*, 7516–7521.
Woodbury, N. W., Peloquin, J. M., Alden, R. G., Lin, X., Lin, S., Taguchi, A. K. W., Williams, J. C., & Allen, J. P. (1994) *Biochemistry* (following paper in this issue).
Wraight, C. A., & Clayton, R. K. (1973) *Biochim. Biophys. Acta 333*, 246–260.